Cell Reports
Article

Mitochondria Coordinate Sites of Axon Branching through Localized Intra-axonal Protein Synthesis

Mirela Spillane,[1] Andrea Ketschek,[1] Tanuja T. Merianda,[2] Jeffery L. Twiss,[3] and Gianluca Gallo[1,*]
[1]Department of Anatomy and Cell Biology, Shriners Hospitals Pediatric Research Center, Temple University, 3500 North Broad Street, Philadelphia, PA 19140, USA
[2]Department of Neurobiology and Anatomy, Drexel University College of Medicine, 2900 Queen Lane, Philadelphia, PA 19210, USA
[3]Department of Biological Sciences, University of South Carolina, 715 Sumter Street, Columbia, SC 29208, USA
*Correspondence: gianluca.gallo@temple.edu
http://dx.doi.org/10.1016/j.celrep.2013.11.022

SUMMARY

The branching of axons is a fundamental aspect of nervous system development and neuroplasticity. We report that branching of sensory axons in the presence of nerve growth factor (NGF) occurs at sites populated by stalled mitochondria. Translational machinery targets to presumptive branching sites, followed by recruitment of mitochondria to these sites. The mitochondria promote branching through ATP generation and the determination of localized hot spots of active axonal mRNA translation, which contribute to actin-dependent aspects of branching. In contrast, mitochondria do not have a role in the regulation of the microtubule cytoskeleton during NGF-induced branching. Collectively, these observations indicate that sensory axons exhibit multiple potential sites of translation, defined by presence of translational machinery, but active translation occurs following the stalling and respiration of mitochondria at these potential sites of translation. This study reveals a local role for axonal mitochondria in the regulation of the actin cytoskeleton and axonal mRNA translation underlying branching.

INTRODUCTION

The formation of axon branches underlies the development of complex patterns of neuronal connectivity and contributes to both adaptive and maladaptive neuroplasticity following nervous system injury in adults (Gibson and Ma, 2011; Onifer et al., 2011). De novo branch formation from the axon shaft requires localized reorganization of the cytoskeleton (Gallo, 2011). The formation of axon branches commences with the emergence of axonal filopodia, which arise from precursor axonal actin patches (Gallo, 2013). In sensory axons, nerve growth factor (NGF) promotes filopodia formation and branching through the intra-axonal protein synthesis of cytoskeletal proteins (Willis et al., 2007; Spillane et al., 2012), which is required for NGF to increase the rate of actin patch formation. NGF also induces a strong correlation between sites of axonal actin patch formation and stalled mitochondria (Ketschek and Gallo, 2010). Although axons generate many filopodia, only a subset mature into branches (Gallo, 2011, 2013), and the mechanism that drives the maturation of a filopodium into a branch remains minimally understood.

Axonal protein synthesis has been implicated in axon guidance, maintenance, regeneration, and branching (reviewed in Hörnberg and Holt, 2013). mRNAs synthesized in the cell body undergo transport into axons incorporated into ribonucleoprotein (RNP) complexes. Extracellular signals promote the transport of RNPs into axons and drive axonal mRNA translation through the release of mRNAs from RNPs and the activation of translational machinery. Whereas much has been learned about the molecular mechanisms of axonal protein synthesis, the organization of the axonal translational system has received less attention. Indeed, the degree of spatial localization of axonal translation is not clear. This study presents evidence that the respiration of stalled axonal mitochondria promotes the maturation of axonal filopodia into branches and generates hot spots of localized mRNA translation.

RESULTS

Stalled Mitochondria along the Axon Correlate with Sites of Protrusive Activity and Branch Maturation

The first step in axon branching is the formation of axonal filopodia (for reviews, see Gallo, 2011, 2013). Second, the entry of microtubules originating in the axon shaft into the filopodia is required, but not sufficient. The final and minimally understood step involves the maturation of the filopodium into a branch. In vitro, this is characterized by the loss of filopodial morphology and the commencement of dynamic rearrangements involving the phase-contrast darkening and thickening of the filopodium, representative of cytoplasmic invasion, and the emergence of filopodia and/or lamellipodia from the microtubule-containing maturing branch (Figures 1A and S1A–S1C; Gallo, 2011; Spillane et al., 2012).

NGF induces axonal protein-synthesis-dependent formation of axonal actin patches, filopodia, and branching (Spillane et al., 2012), effects which are maximal at 30 min posttreatment.

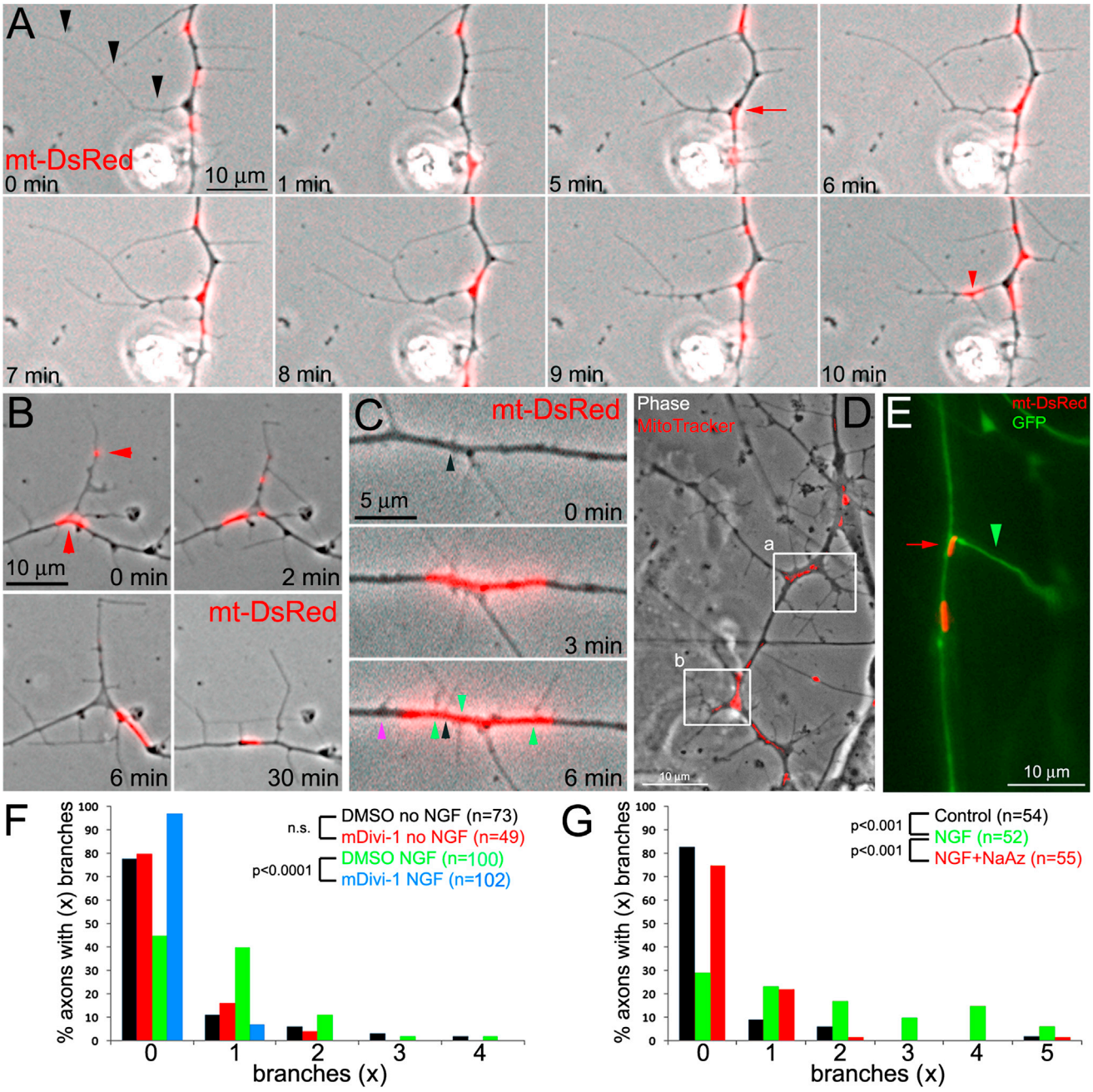

Figure 1. Axonal Mitochondria Stall at Sites of Branch Maturation

(A) Phase contrast imaging of mt-DsRed-expressing axons. A mitochondrion (red arrow at 5 min) stalls at the base of a previously stable filopodium (arrowheads at 0 min). This event correlates with the phase darkening of the filopodial base and the initiation of lateral protrusions along the shaft of the filopodium. By 10 min, the filopodium has reorganized into a dynamic maturing branch containing a mitochondrion (red arrowhead at 10 min). Considering all cases of mitochondria stalling at the base of filopodia for greater than 4 min, 30% matured into branches (n = 59). Mitochondria stalling at the base of stable filopodia, previously not engaging in protrusive tip activity, resulted in cycles of protrusive tip activity in 72% of cases (n = 59; Figure S2A), regardless of whether the filopodium eventually matured into a branch. Considering filopodia experiencing mitochondria stalling events lasting less than 15 min and comparing to filopodia from the same axons which persisted a minimum of 15 min and did not exhibit mitochondria stalling for more than 2 min, 54% and 26%, respectively, exhibited cycle of tip protrusive activity ($p < 0.001$; Fisher's exact test).

(B) Mitochondria are present at the base and within the shaft of this nascent branch (0 min, arrowheads). By 6 min, the mitochondria have departed from the branch, and by 30 min, the branch has resumed the appearance of a filopodium.

(C) Prior to arrival of the mitochondrion, between 2 and 3 min, the axon exhibited a filopodium which is maintained throughout the sequence (black arrowhead). Between 3 and 6 min, the segment of the axon populated by the mitochondrion gives rise to three filopodia (green arrowheads denote the location of the bases of

(legend continued on next page)

We performed live imaging of chicken embryonic sensory neurons transfected with mitochondrially targeted DsRed (mt-DsRed; Nasr et al., 2008) for a period of 60 min starting 30 min after bath application of NGF (n = 19 axons). We observed that previously stable filopodia underwent maturation when one or more mitochondria stalled at their base for a minimum period of 4 min (Figure 1A). Out of 13 cases in which mitochondria persisted at the base of a filopodium for greater than 20 min, all 13 underwent maturation into a branch. We also observed six cases in which mitochondria departed from the base of branches that begun maturing prior to the commencement of the time lapse. Following 4–11 min of the departure of mitochondria, the branches begun to wither and resumed a more linear and thin filopodial morphology (Figure 1B). Furthermore, 81% of newly formed filopodia emerged from sites where mitochondria underwent temporary stalling for >2 min (Figure 1C). These observations reveal a relationship between mitochondria positioning and axonal actin-dependent protrusive activity.

The distribution of mitochondria in relation to axon branches was also addressed by labeling with Mitotracker dyes. In the presence of NGF, 84% (n = 72) of axonal branching sites exhibited one or more mitochondria (Figure 1D), and branches greater than 25 μm in length invariably contained one or more mitochondria. The endoplasmic reticulum was also found to colocalize with mitochondria at sites of branching (Figures S1D–S1F). Furthermore, we assessed the relationship between sites of axon branching and mitochondria in an acute living embryonic spinal cord explant preparation, as previously described (Spillane et al., 2011, 2012; Donnelly et al., 2013), by electroporating chicken embryo sensory neurons in vivo with GFP and mt-DsRed. Within the spinal cord, 78% (n = 127) of axon branching sites exhibited mitochondria at their base (Figure 1E), and mitochondria were also observed within 21% of branches.

Manipulation of Axonal Mitochondria Content and Respiration Impair Axon Branching

To functionally address whether mitochondria contribute to branching, we depleted the axons of mitochondria using a chronic treatment with mDivi-1. mDivi-1 is an inhibitor of the dynamin-1-like protein (DRP1) guanosine triphosphatase, required for mitochondria fission, and decreases the density of mitochondria in the axon (Steketee et al., 2012). DRP1 has been previously shown to specifically localize to mitochondria in the axons of chicken sensory neurons (Amiri and Hollenbeck, 2008). Consistent with Steketee et al. (2012), mDivi-1 decreased the density of axonal mitochondria labeled with Mitotracker by 50%–60%, and mitochondria also exhibited a 53% decrease in length (Figures S2B and S2C). Axons raised in the presence of mDivi-1 and NGF exhibited a pronounced decrease in the number of axon branches relative to cultures treated with vehicle control and NGF (Figure 1F). Notably, mDivi-1 treatment did not alter the already low level of baseline branching in the absence of NGF. To determine if the respiration of axonal mitochondria is required for NGF-induced branching, neurons were cultured overnight without NGF and then severed from the cell bodies just prior to treatment with NGF (as in Spillane et al., 2012) with or without treatment with inhibitors of respiration. Inhibition of mitochondrial respiration in conjunction with an acute 30 min treatment with NGF blocked branching (Figures 1G, S2D, and S2E).

Inhibition of Mitochondrial Respiration and Protein Synthesis Impair the Maturation of Branches at Sites with Stalled Mitochondria

To more directly address the role of mitochondria in the dynamics of branching, we inhibited mitochondrial respiration in neurons transfected with mt-DsRed starting at 20 min following NGF treatment and obtained videos starting 10 min later for the next hour, as performed in Figure 1A. Under these conditions, 79% of mitochondria were stalled for greater than a 20 min period in contrast to 22% in control conditions (Figure 2A), consistent with the recent report that inhibition of respiration stalls mitochondria (Zala et al., 2013). Although mitochondria stalled, filopodia did not mature into branches when respiration was inhibited (Figure 2A). Only 2% (n = 116) of filopodia with mitochondria stalled for greater than 20 min at their base exhibited some degree of maturation (n = 14 axons). This is in contrast to control conditions in which mitochondria stalling at the base of filopodia for greater than 20 min resulted in branch maturation in 13/13 cases.

We next determined the effects of inhibiting protein synthesis, which we previously showed blocks NGF-induced increases in the formation of actin patches, filopodia, and branches (Spillane et al., 2012), on the maturation of stable filopodia associated with stalled mitochondria into branches. In cultures treated with the translational inhibitor cycloheximide (35 μM) in conjunction with NGF, 11% of mitochondria-stalling events longer than 20 min (range 20–60 min) resulted in maturation (n = 18; Figure S2F), compared to 100% in controls (n = 13). These results indicate that protein synthesis contributes to branch maturation.

CALI Ablation of Mitochondria Locally Impairs Filopodial Dynamics, Branch Formation, and Maintenance

Killer Red (KR) is a fluorescent protein that upon illumination generates 1,000-fold greater level of reactive oxygen species (ROS)

new filopodia). A filopodium also arises a few microns to the left of the mitochondrion (purple arrowhead). Only filopodia directly colocalizing with mitochondria were considered in the quantitative analysis.

(D) Mitotracker-labeled mitochondria aggregate at the base of established branches (a) and nascent branches (b).

(E) Example of mt-DsRed-labeled mitochondria in an axon cotransfected with GFP and imaged in an acutely explanted embryonic spinal cord at 100×. Note the mitochondrion (red arrowhead) at the base of the branch (green arrowhead). The tip of the branch ends in a different focal plane.

(F) Distribution of axons with (x) branches along the distal 100 μm of axons. Explant ganglion cultures were raised in mDivi-1 (20 μM) or DMSO overnight, with or without 40 ng/ml NGF. In the absence of NGF, mDivi-1 did not alter branching. However, mDivi-1 prevented the increase in branches induced by NGF.

(G) Axons were severed from the cell bodies just prior to treatment with NGF. A 30 min treatment with 40 ng/ml NGF induced pronounced branching. The NGF induction of branches was blocked by a 15 min pretreatment with the respiration inhibitor sodium azide (NaAz; 25 mM). For (F) and (G) four to six cultures were analyzed per group. The number of branches in the distal 100 μm of axons was determined. n = axons. In (F) and (G), raw categorical data were analyzed using X^2 test.

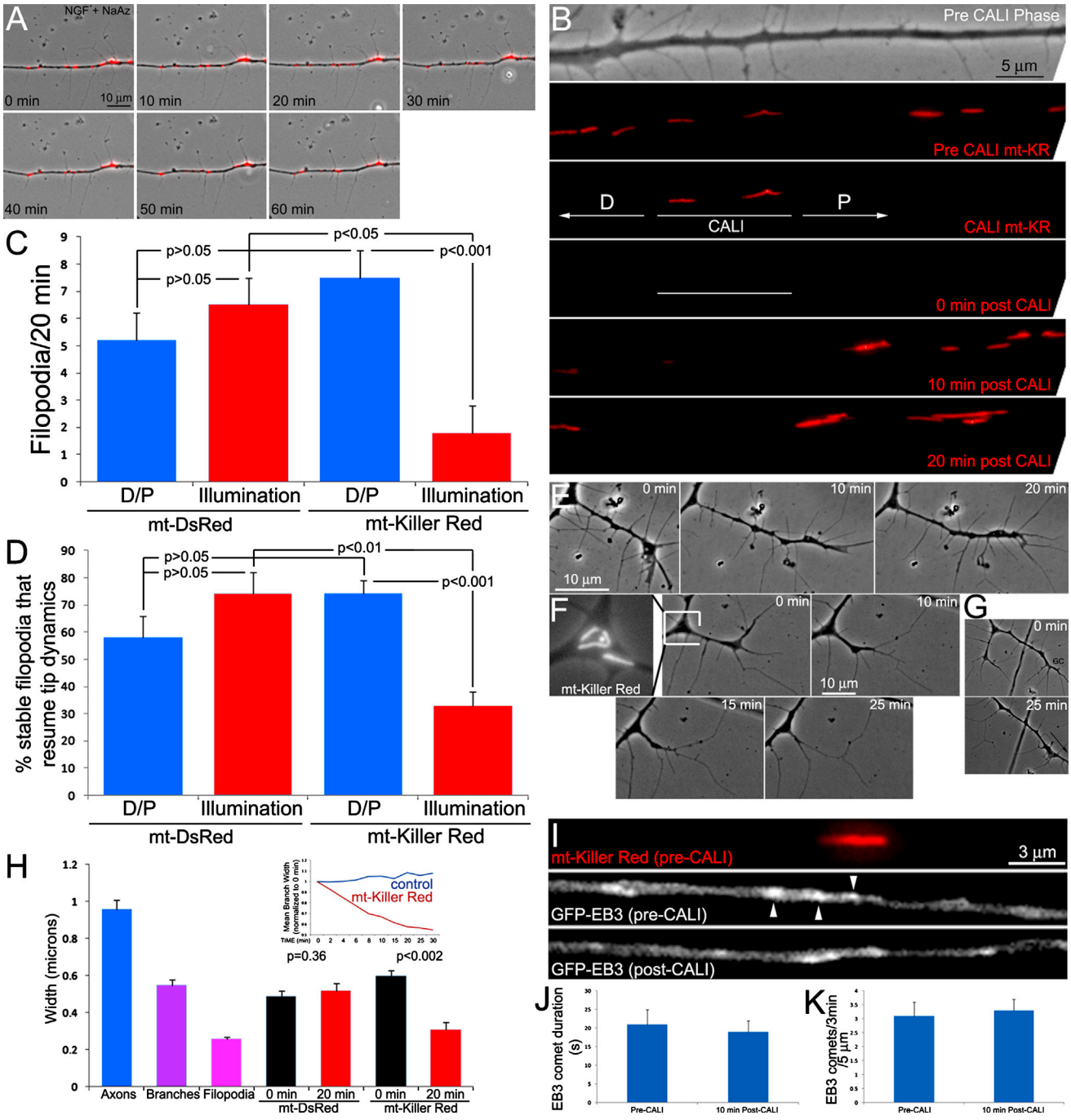

Figure 2. Effects of Inhibiting Mitochondrial Respiration and Mitochondria Ablation on Axonal Protrusive Dynamics

(A) Example of axonal protrusive dynamics in an axon treated with NGF for 20 min and then with NaAz (25 mM) 10 min prior to the beginning of imaging and subsequently tracked for 60 min. Note that mitochondria are mostly stalled, but the stalling in the absence of respiration does not correlate with branch maturation or filopodial dynamics.

(B) Example of CALI of mitochondrially targeted killer red (mt-KR) along axons. The distal (D) and proximal (P) segments, adjacent to the CALI segment, used in the quantitative analysis are also shown. The CALI and 0 min post-CALI panels are shown with only the CALI region illuminated.

(C) CALI of mt-KR results in decreased rates of filopodial formation. Kruskal-Wallis ANOVA with Dunn's post hoc tests. n = 15 axons/group.

(D) CALI of mt-KR results in decreased percentages of stable filopodia that resume tip dynamics. ANOVA with Bonferroni's post hoc tests.

(E) Example of a control CALI-illuminated branch. The branch appears unaffected and grows during the imaging period.

(F) The leftmost panel shows the base of the branch during CALI and the overlaid mt-KR signal. During the subsequent 20 min, the branch withers and attains a filopodial morphology.

(legend continued on next page)

than other fluorescent proteins (Bulina et al., 2006). When KR is targeted to the inner membrane of the mitochondrion, illumination at 545 nm results in the ablation of the mitochondrion due to localized intramitochondrial ROS damage (Bulina et al., 2006). We locally ablated mitochondria in 15–20 μm segments of axons and tracked filopodial dynamics in these segments relative to same-sized adjacent segments of the axons (see Supplemental Information). Illumination of mt-DsRed served as a control. Positive controls in neurons expressing mitochondrial KR (mt-KR) and mitochondrial GFP (mt-GFP) revealed that chromophore-assisted light inactivation (CALI) of mt-KR resulted in shrinkage of axonal mitochondria and stopped the transport of mitochondria subjected to CALI without preventing the transport of new mitochondria into axons subjected to CALI (Figures S3A–S3D). CALI of mitochondria decreased the initiation of new filopodia, and the resumption of tip dynamics by previously stable filopodia, in illuminated segments of axons (Figures 2B–2D). However, this did not affect the morphology or width of the axon shaft at 20 min post-CALI relative to preablation images (Wilcoxon matched-pairs signed-ranks test; $p = 0.45$). Illumination of mt-DsRed-labeled mitochondria had no effect on filopodial dynamics (Figures 2C and 2D). Analysis of the frequency of filopodia maturation into a branch between illuminated and nonilluminated segments of mt-KR-expressing axons showed no maturation events in the illuminated segments (0/15) relative to seven events in the adjacent size-matched segments (7/30; Fisher's exact test; one-tailed $0 = 0.019$).

The spontaneous departure of mitochondria from sites of branching correlates with the withering of the branch back to a filopodial morphology (Figure 1B). CALI of mitochondria at the base of branches 10–30 μm in length resulted in a similar withering of branches, as reflected by changes in the width of the branches, which attained filopodial morphology and width by 20–30 min following CALI (Figures 2E–2H). Collectively, these CALI experiments indicate that the observed correlations between mitochondria positioning and the dynamics of axonal filopodia and branches are indicative of a role of mitochondria.

Inhibition of Mitochondrial Function Does Not Disrupt the Axonal Microtubule Cytoskeleton

The invasion of filopodia by microtubules is required for branching, and NGF promotes microtubule polymerization and targeting into axonal filopodia independent of intra-axonal protein synthesis (Spillane et al., 2012). Analysis of GFP-end-binding protein 3 (EB3) comets, reflective of polymerizing microtubule tips (Ketschek and Gallo, 2010), in axon segments populated by mitochondria before and after mt-KR CALI did not reveal changes in the number or duration of comets (Figures 2I–2K), indicating the CALI of mitochondria did not affect microtubule tip dynamics. Inhibition of respiration did not change the percentage of filopodia containing microtubules and similarly did not affect the microtubule content of axons (Figures S3E–S3H).

Axons Exhibit Hot Spots of mRNA Translation Determined by the Positioning and Respiration of Stalled Mitochondria

The 3′ UTRs of mRNAs contain the motifs that target their transport into axons (Vuppalanchi et al., 2009). The axonal translation of individual mRNA species can be visualized through the expression of constructs containing the 3′ UTR of the mRNA of interest with the open reading frame of GFP containing a myristoylation (myr) sequence (Aakalu et al., 2001). Cotranslational myristoylation targets GFP to the nearby plasma membrane, subsequently restricting its diffusion (Aakalu et al., 2001; Yudin et al., 2008). Fluorescence recovery after photobleaching (FRAP) ± translational inhibitors is then used to determine the extent of translation. Thus, in this system, myrGFP serves as a reporter for the temporal and spatial aspects of cellular translation.

NGF drives the axonal synthesis of cortactin, actin-related protein 2 (Arp2), and β-actin (Willis et al., 2007; Spillane et al., 2012). The distribution of myrGFP in axons expressing myrGFP constructs with the 3′ UTRs of β-actin, cortactin, and Arp2 prior to photobleaching was noted to be heterogeneous and exhibit hot spots (Figures 3A and S4A). These hot spots do not correlate with volumetric variations, do not contain accumulations of mCherry targeted to the membrane using a CAAX domain (Yu and Bement, 2007), and are not evident in axons expressing myrGFP with the 3′ UTR of γ-actin, a nonaxonally targeted mRNA (Figures S4B–S4D). Figure 3A shows an example of the axonal expression pattern of myrGFP mRNA targeted into axons using the 3′ UTR of β-actin. Figure 3B provides an example of the ratiometric analysis (yielding the value R) of myrGFP relative to soluble red fluorescent protein (RFP), the volumetric baseline (Figure S4B). In FRAP studies, we observed that following photobleaching fluorescence recovered initially at sites containing previous hot spots (Figure 3C). We also observed the formation of new hot spots in locations not previously populated by hot spots and that some hot spots present prior to photobleaching did not recover (Figure 3C).

We next determined the localization of myrGFP hotspots relative to axon branches and mitochondria. In neurons cultured overnight, the location of myrGFP hotspots, generated from mRNAs with the axonally targeting 3′ UTRs described above,

(G) The same axon as in (F) is shown tracking the growth cone over a 25 min period (rotated relative to F). The growth cone continues to advance and by 25 min has grown out of the field of view indicating no adverse effects.
(H) CALI of mt-KR at the base of branches causes a progressive decrease in width. The three leftmost bars show mean widths of axons, branches, and filopodia as determined by morphological criteria. The black and red bars show the width of branches as a function of illumination and mt-KR/mt-DsRed expression at 0–20 min. The mt-KR branches attain a width in the range of filopodia whereas the control branches maintain their width. The inset shows the change in mean width of branches as a function of time. Wilcoxon matched-pairs signed-ranks test. $n = 11$ axons per group. $n = 50$ for filopodial width in third bar from the left.
(I) Examples of a CALI mt-KR axon segment with the target mitochondrion and EB3 comet examples. EB3 comets in stills appear as bright puncta (arrowheads).
(J) CALI did not affect EB3 comet duration.
(K) CALI did not affect frequency of comets. For both (J) and (K), $n = 12$ axons ($p > 0.05$ for both J and K, paired t test). Post-CALI imaging started at 10 min post. Three-minute sampling at 3 s intervals.
In (C), (D), (H), (J), and (K), mean and SEM are shown.

Cell PRESS
Open ACCESS

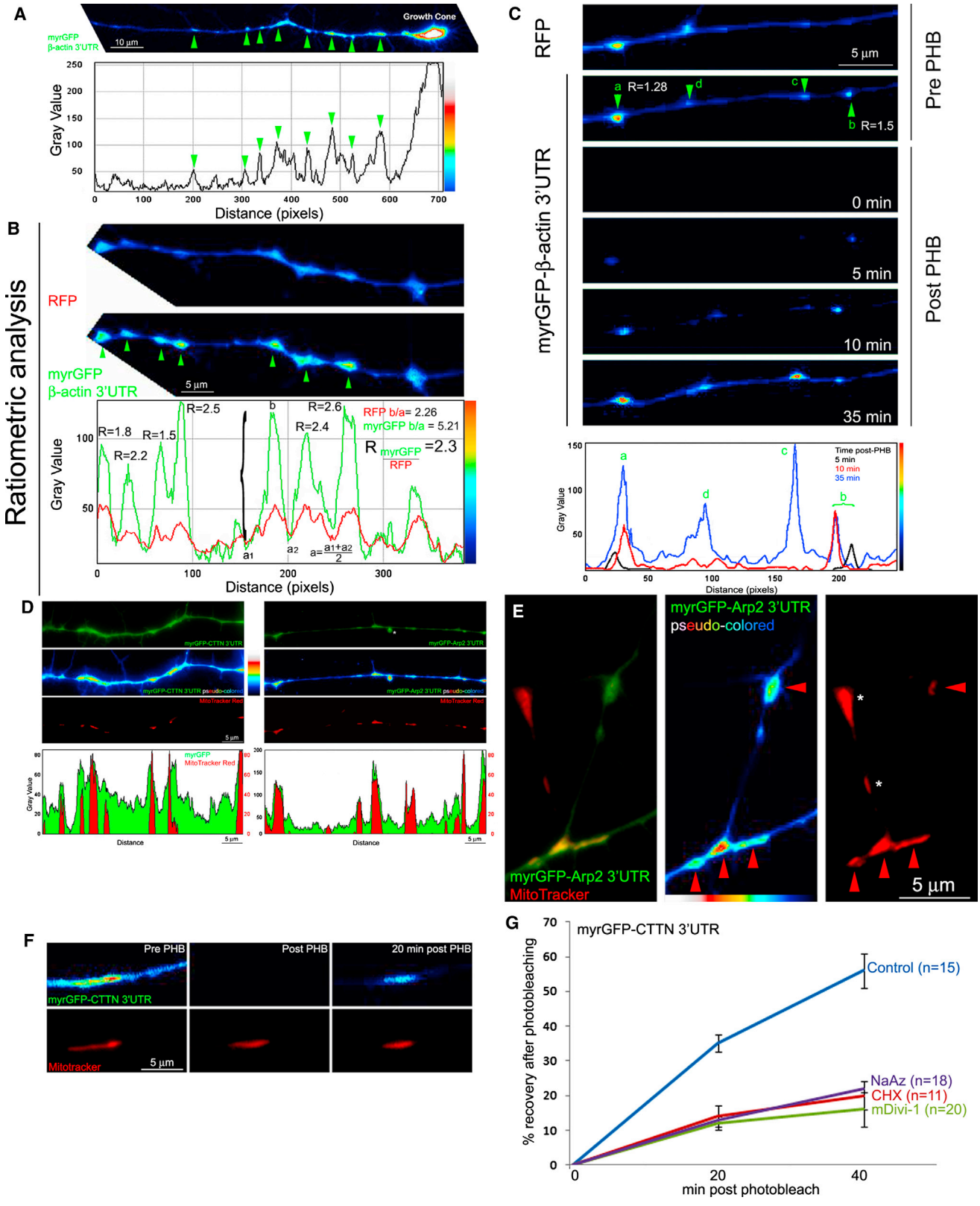

(legend on next page)

correlated strongly with Mitotracker-labeled mitochondria (Figure 3D). In contrast, no colocalization of myrGFP accumulation with mitochondria was noted when myrGFP was expressed from the nonaxonally targeting construct containing the 3′ UTR of γ-actin (Figure S4E). For all three axonally targeted 3′ UTR constructs, myrGFP hot spots were present at the base of branches that also contained mitochondria at their base (Figure 3E). In nonneuronal cells, myrGFP did not accumulate on mitochondria (Figure S4F).

In order to analyze directly whether myrGFP hot spots form preferentially at sites populated by mitochondria, we performed FRAP analysis in axons with labeled mitochondria. FRAP analysis of myrGFP-cortactin 3′ UTR-expressing axons, labeled with Mitotracker, showed that 74% of hot spots associated with a mitochondrion showed recovery from photobleaching if the mitochondrion remained in situ over the 20 min postbleaching observation period (n = 31 hot spots, 14 axons; Figure 3F). Similarly, FRAP analysis of axons expressing myrGFP-β-actin 3′ UTR cotransfected with mt-DsRed revealed that 60% of hot spots (n = 74 hot spots, 17 axons) reformed during the first 20 min of imaging were associated with mitochondria in situ (Figure S5A). These observations indicate that the colocalization of myrGFP hot spots and mitochondria reflects preferential translation of myrGFP in the vicinity of mitochondria.

To experimentally address the role of mitochondria and their respiration in the translation of these mRNAs, FRAP was performed using the respiration inhibitors sodium azide (NaAz) and antimycin-A. FRAP analysis revealed that inhibition of mitochondrial respiration prevented recovery of myrGFP-cortactin 3′ UTR (Figure 3G). Similarly, inhibition of respiration prevented fluorescence recovery and hot spot reformation of myrGFP constructs with the 3′ UTRs of β-actin, Arp2, and cortactin (Figures S5B–S5E). To directly address the requirement of individual mitochondria in the formation of translational hot spots, we used CALI of mt-KR to ablate mitochondria in the axons of neurons transfected with myrGFP-cortactin 3′ UTR. CALI of mitochondria impaired hotspot formation in illuminated axon segments relative to nonilluminated locations along the same axons (Figures 4A and 4C). Control illumination of mt-DsRed mitochondria did not affect hot spot recovery (Figures 4B and 4C). In mDivi-1-treated axons, although net recovery was largely inhibited (Figure 3G), we did observe that when myrGFP signal recovered it occurred at sites populated by mitochondria (Figure S5F), as in control conditions.

Relationship of Translational Machinery to Axonal Filopodia, Branches, and Mitochondria

In order to visualize the localization of ribosomes in axons, we expressed the ribosomal protein L10A (GFP) and performed total internal fluorescence (TIRF) microscopy. Using wide-field microscopy, expression of L10A produced a relatively homogeneous signal with occasional puncta and accumulations (not shown). In contrast, and consistent with the notion that in axons ribosomes are targeted to regions adjacent to the plasma membrane (Alvarez et al., 2000), TIRF imaging revealed small puncta of L10A along axons (Figure 5A). Some puncta underwent bidirectional transport along the axon (Figure S6A). L10A puncta were detectable at the base of 72% of filopodia (n = 10 axons) and in regions of axons enriched in actin filaments (Figure 5A). As an alternative method to detect ribosomes, we stained with the Y10B antibody to ribosomal 5.8S RNA, which in the cytoplasm is only found associated with ribosomes and specifically labels ribosomes in chicken neurons (Garden et al., 1995). Similar to the pattern of L10A, Y10B staining revealed small puncta of staining along the axon shaft, which were concentrated in axonal domains containing multiple filopodia and at the base of branches (Figures 5B and 5C).

The axonal targeting of β-actin mRNA promotes branching and filopodia formation (Donnelly et al., 2013). β-actin zipcode-binding protein 1 (ZBP1) is a component of RNPs that carry β-actin mRNA into axons and regulates its translation (Gu et al., 2002). Overexpression of ZBP1 increased the proportion

Figure 3. Mitochondria Determine Sites of Preferential Axonal mRNA Translation

(A) Example of myrGFP expressed in axons using the 3′ UTR of β-actin. Corresponding line scan of the myrGFP signal with apparent local accumulations denoted by green arrowheads.

(B) Ratiometric analysis of myrGFP accumulation relative to volume (RFP). Line scans for both myrGFP and RFP are shown below the pictures. An example of the ratiometric value (R), determined by the formula shown in the image, representing the hot spot marked by the {. Briefly, the intensity of the peak of the myrGFP signal (b) is divided by the mean of the troughs of the signal in the line scan (a1, a2). Using the same x axis positions on the line scan, the same value is obtained for RFP. The value obtained for myrGFP is then divided by that for RFP, yielding R. R = 1.0 reflects codistribution of the reporters, as observed with RFP and GFP (Figure S4). We considered R > 1.25 to be a hot spot. R values for the myrGFP peaks are shown.

(C) Four hot spots (a–d) are shown representing the variety of FRAP recoveries observed (PHB, photobleach). Hot spot (a) recovers in situ. Hot spot (b) recovers with an apparent slight movement. Although the myrGFP accumulations (c and d) were initially below the ratiometric threshold (R) of 1.25, the location of accumulation of (c) undergoes a localized increase in intensity. The location of hot spot (d) also undergoes some recovery. The line scan below shows the local changes in intensities of the myrGFP signal color coded as a function of time.

(D) Apparent myrGFP hot spots colocalize with mitochondria in axons. Line scans of the myrGFP and Mitotracker intensity are shown below the images. Note that peaks in myrGFP correlate with mitochondria (CTTN, cortactin). 91% (n = 88 hot spots, 40 axons), 89% (n = 82, 38), and 85% (n = 62, 26) of hot spots colocalized with mitochondria for myrGFP constructs with the β-actin, Arp2, and cortactin 3′ UTRs, respectively. However, not all mitochondria were associated with myrGFP hot spots; 57% (n = 140 mitochondria), 52% (n = 140), and 59% (n = 90) of mitochondria exhibited hot spots, respectively. Thus, the majority of hot spots colocalize with mitochondria, but not all mitochondria exhibit hot spots.

(E) Example of colocalization of myrGFP hot spots with the bases of branches and accompanying mitochondria (red arrowheads). The mitochondria labeled by the asterisk belong to a nontransfected axon.

(F) Example of the recovery of a myrGFP-cortactin (CTTN) 3′ UTR hot spot following FRAP at a site containing a stalled mitochondrion (Mitotracker labeled). 16% of hotspots did not exhibit recovery, even if the mitochondrion remained in place, and 10% appeared in a new position correlating with a mitochondrion.

(G) Quantitative FRAP analysis of myrGFP translation (3′ UTR of cortactin). Both a 10 min pretreatment with sodium azide (NaAz, 25 mM) and chronic mDivi-1 (20 μM) treatment inhibit FRAP ($p < 0.01$ for both comparisons to control; Welch t test). The effects of a 10 min pretreatment with the translational inhibitor cycloheximide (35 μM) is also shown for comparison (also see Spillane et al., 2012). Means and SEMs are shown.

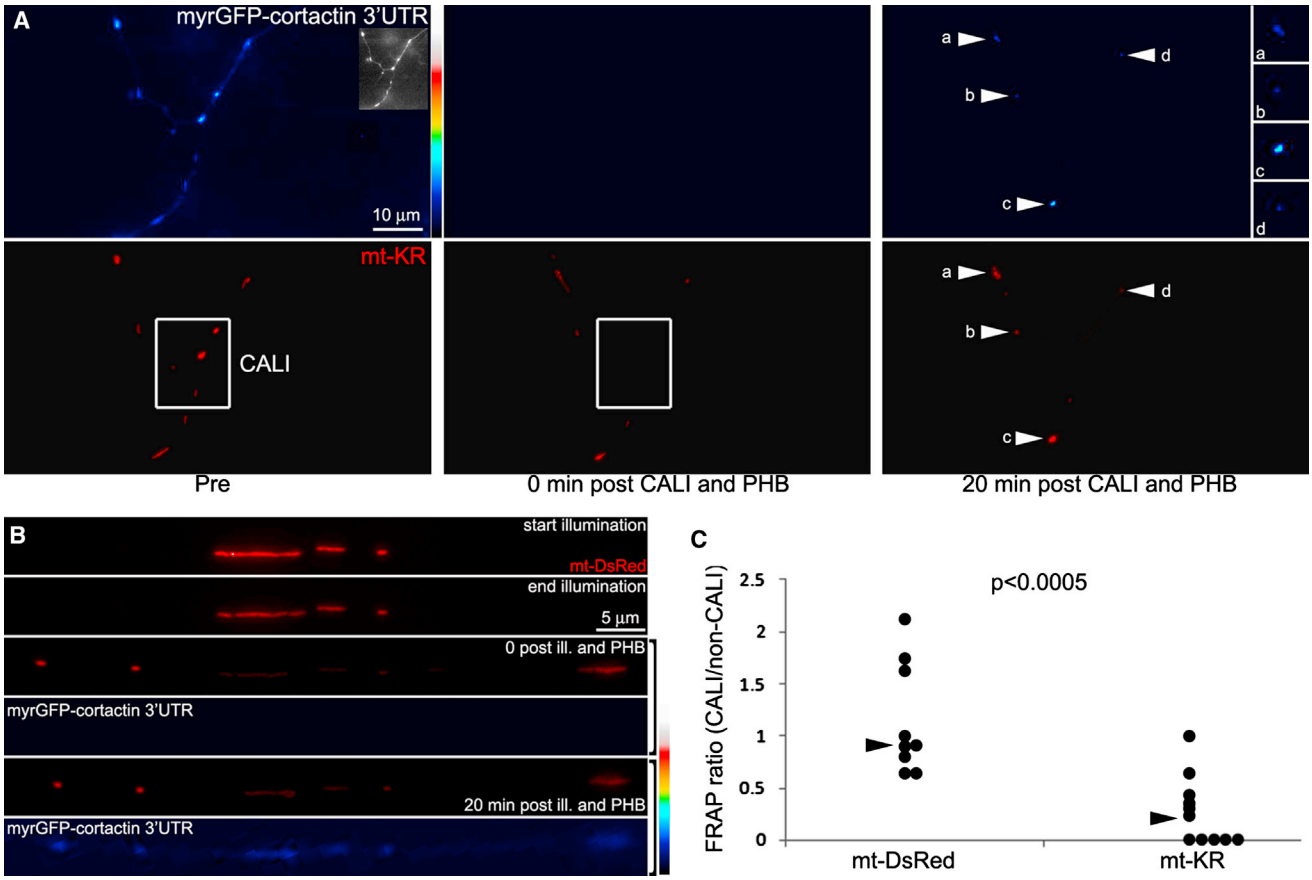

Figure 4. CALI of mt-KR Locally Impairs myrGFP-Cortactin 3′ UTR Hot Spot Recovery following PHB

(A) Example of a branched axon (morphology shown in inset) which underwent CALI in the boxed region. By 20 min, mitochondria outside the CALI region labeled a–d undergo recovery of myrGFP. In the myrGFP panel at 20 min, the hot spots associated with mitochondria a–d are shown as magnified insets. Minimal to no recovery is observed associated with the four mitochondria in the CALI region (see box in the Pre panels).

(B) Example of myrGFP recovery in control mt-DsRed-expressing axon. Top panels show mitochondria in the control-CALI illumination area at the start and end of illumination (ill.), note decrease in DsRed intensity. In register panels showing mitochondria and myrGFP signal at 0–20 min post-PHB.

(C) Quantification of hot spot recovery at sites populated by mitochondria in CALI versus non-CALI regions of the same axon. A ratio of 1.0 indicates no difference, whereas a ratio lower than 1.0 reflects lower recovery in the CALI region. For details on the metric, see Supplemental Information. The arrowheads denote the median, and each dot represents one axon. Mann-Whitney test.

of axons undergoing branching and the number of axon branches along distal axons relative to controls by 61% (Figure 5D; n = 69, 41 axons; p = 0.001, X^2 test on distributions as in Figure 1; p < 0.02, comparing number of branches/unit length axon, Mann-Whitney test). As determined by live imaging, the distribution of mCherry-ZBP1 in axons was punctate with both stable and moving puncta, as previously reported (Zhang et al., 2001). ZBP1 particles often localized to the base of filopodia, and ZBP1 was clearly enriched at branch points (Figures 5E and 5F). Time-lapse imaging revealed that 75% of filopodia (n = 28 filopodia, 14 axons) arose from sites populated by ZBP1 particles, and ZBP1 also exhibited dynamic localization into filopodial shafts (Figure 5G). Analysis of mitochondria and ZBP1 dynamics in axons (Figure 5H) revealed that 79% of transported mitochondria that subsequently stalled for greater than 2 min (n = 14 mitochondria, 12 axons) stalled within axon segments already populated by ZBP1 particles at the base of filopodia. Finally, we used fluorescence in situ hybridization (FISH) to determine if a ZBP1 cargo mRNA might also localize to these sites. β-actin mRNA granules detected by FISH were present at 73% of sites populated by mitochondria (35 axons, 145 mitochondria; Figure 5I). We also note that mRNAs for nuclear encoded mitochondrial proteins have also been localized to axonal mitochondria (Aschrafi et al., 2010). These data indicate that endogenous mRNAs are also translated in close proximity to the stalled mitochondria adjacent to developing axonal branches.

DISCUSSION

The axon is the only cellular domain that reaches distances of up to meters from the cell body. The transport of membranous compartments and proteins into axons and the intra-axonal synthesis of proteins are the two major mechanisms known to

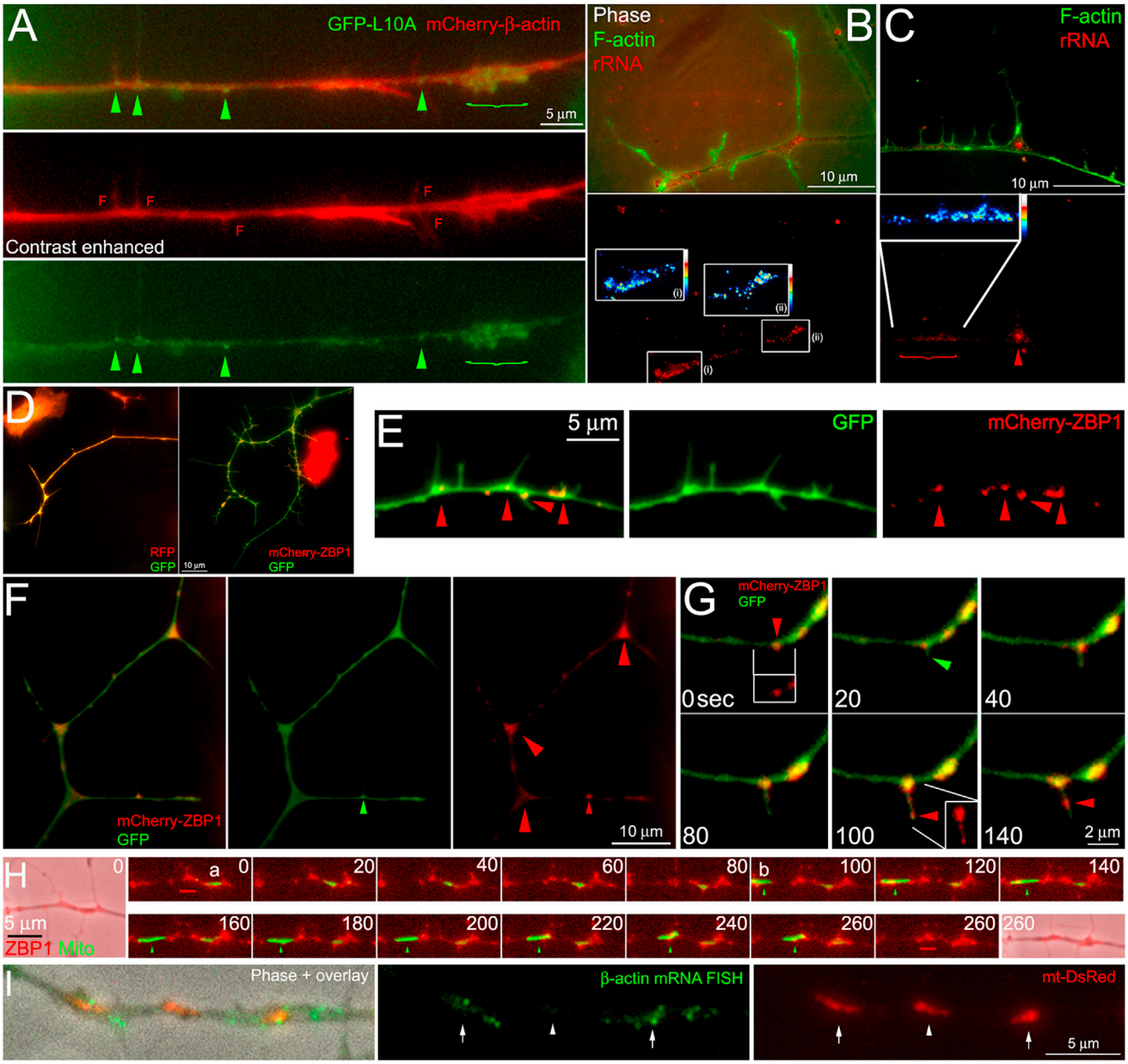

Figure 5. Localization and Dynamics of Branching Related Translational Machinery in Axons

(A) TIRF imaging of an L10A-GFP-expressing neuron cotransfected with mCherry-β-actin. Puncta of L10A (green arrowheads) are observed at the bases of filopodia (F) and actin-enriched axonal domains. The panel showing the mCherry-β-actin signal alone is contrast enhanced to facilitate visualization of filopodia. The region denoted by { shows a lamellipodia-like protrusion, enriched in L10A.

(B) Example of Y10B staining at two branch points (i and ii). False-colored magnified insets of (i and ii) are shown in lower panel. The number of puncta in 5 μm segments of the axon, centered on the branch point, was 149% of that in adjacent 5 μm segments not containing branching sites ($p < 0.001$; $n = 32$ branch points; Welch t test).

(C) Accumulation of Y10B stain along segments of the axon with multiple filopodia ({) and branch points (arrowhead). Inset shows false-colored magnified view of ({).

(D) Overexpression of mCherry-ZBP1, and cotransfection with GFP, increases the numbers of axonal filopodia and branches relative to neurons cotransfected with RFP and GFP.

(E) mCherry-ZBP1 particles (red arrowheads) associate with the base of filopodia.

(F) mCherry-ZBP1 accumulates at branch points (large arrowheads). The small arrowhead denotes a ZBP1 particle in the branch correlating with the base of a filopodium.

(G) mCherry-ZBP1 particles that did not move during imaging (0 s, red arrowhead; inset) were associated with sites of filopodial emergence (20 s, green arrowhead). Particulate mCherry-ZBP1 was also observed to enter filopodial shafts (100–140 s, red arrowhead; inset).

(legend continued on next page)

support and maintain axonal morphology and function. This study indicates that axonal mitochondria contribute significantly to axonal protein synthesis and determine sites of greatest synthesis along axons. Many axonal pathologies involve mitochondrial malfunction (Mattson et al., 2008), and mitochondrial dysfunction downstream of the inability to synthesize lamin B protein in axons induces degeneration of embryonic axons (Yoon et al., 2012). Thus, impairment of axonal protein synthesis downstream of mitochondrial malfunction may also underlie aspects of diseases.

The branching of axons is of primary importance to the formation of complex neuronal circuitry during development (Gallo, 2011) and to the endogenous repair mechanisms of the nervous system (Onifer et al., 2011). Axon branching requires axonal mRNA translation (Spillane et al., 2012; Hörnberg et al., 2013; Kalous et al., 2013) and the stalling of mitochondria (current study; Courchet et al., 2013). The results of the current study suggest a model for the coordination of axonal translational machinery and mitochondria in determining sites of branching and active translation along sensory axons. Translational machinery targets to actin filament enriched domains of the axon, which generate potential sites of translation (also see Sotelo-Silveira et al., 2008). Interestingly, ribosomes and ZBP1 associate through receptor for activated C-kinase (RACK; Ceci et al., 2012), and translational machinery associates with deleted in colorectal cancer receptors (Tcherkezian et al., 2010), indicating molecular mechanisms for the orchestration of multiple elements of the translation system. The formation of preferential sites of active axonal translation is accomplished by the stalling and respiration of mitochondria at previously established potential sites of translation, as exemplified by the stalling of mitochondria at sites already populated by ZBP1. The stalled mitochondria at potential translation sites likely act in concert with localized signaling events to coordinate the spatiotemporal regulation of translation. Indeed, NGF-induced signaling by phosphatidylinositol 3-kinase (PI3K) increases mitochondrial respiration (Verburg and Hollenbeck, 2008), NGF promotes the localized association of PI3K signaling microdomains along axons with actin patches and mitochondria (Ketschek and Gallo, 2010), and NGF also drives axonal translation in the context of axon branching (Spillane et al., 2012). This spatiotemporal coordination generates nodes of localized translational activity, which promote the translation-dependent maturation of filopodia into branches and also contributes to actin dynamics underlying filopodia formation and behavior. The CALI experiments indicate that the role of mitochondria in the regulation of axonal protrusive dynamics and translation is local on a scale of less than 20 μm. The respiration of en passant mitochondria regulates the variability in presynaptic activity (Sun et al., 2013). Thus, we speculate that, whereas stalled mitochondria generate localized hot spots of active translation, motile mitochondria may also support a more diffuse form of axonal translation.

The stalling of mitochondria associated with branching along cortical axons is controlled by liver kinase B1 (LKB1) (Courchet et al., 2013). Interestingly, experimental manipulation of LKB1, or the associated synapses of amphids defective kinase-A (SAD) kinases, does not regulate the development of nociceptive NGF-responsive axons that were studied here (Lilley et al., 2013). However, SAD kinases are involved in the neurotrophin-3-dependent branching of proprioceptive sensory axons (Lilley et al., 2013). We suggest that the PI3K-Akt-mammalian-target-of-rapamycin signaling axis is instead used by nociceptive sensory axons to orchestrate sites of branching in response to NGF (Ketschek and Gallo, 2010; Spillane et al., 2012). The signaling mechanism that stalls mitochondria in sensory axons remains to be fully elucidated, but a prior study indicates that PI3K activity is required for the capture of mitochondria at sites of axons in contact with localized sources of NGF (Chada and Hollenbeck, 2003), which also locally induce branching (Gallo and Letourneau, 1998). Collectively, these studies indicate neurotrophin-specific mechanisms in the regulation of mitochondria targeting and function during the branching of different populations of sensory axons (discussed in Xing et al., 2013).

This study also reveals that the role of mitochondria respiration and associated translation contributes to the actin-, but not microtubule-, dependent component of NGF-induced branching. Microtubules likely promote branching by targeting axonal transport cargoes into nascent branches (e.g., synaptic vesicles; Greif et al., 2013). Interestingly, vesicle transport along microtubules is independent of mitochondrial respiration and requires vesicle-associated glycolysis (Zala et al., 2013). Continued dissection of the bioenergetics of axon branching may reveal additional specific roles for mitochondria respiration and glycolysis.

EXPERIMENTAL PROCEDURES

Neuronal Cultures

Embryonic day 7 chicken dorsal root ganglion neurons were cultured either as dissociated cells, for experiments involving electroporation or dye labeling, or explants (Figures 1F and 1G). All culturing was performed on laminin-coated substrata (25 μg/ml; Invitrogen) in defined F12H (Invitrogen) serum-free medium with supplements as previously described in Spillane et al. (2012), and detailed in Lelkes et al. (2006). NGF (R&D Systems) was used at 40 ng/ml. For the experiment in Figure 1G, axons extending from explants were severed from their cell bodies using a scalpel, as previously described (Spillane et al., 2012), just prior to treatment with NGF. For TIRF imaging, substrata were coated first with polylysine (100 μg/ml) and then laminin to promote the uniform attachment of axons to the substratum and thus provide more uniform imaging.

Electroporation

Dissociated neurons were electroporated using an Amaxa Nucleofector and Amaxa chicken neuron transfection reagents (Lonza), as previously described (Spillane et al., 2011, 2012). In vivo electroporation and preparation of acute spinal cord explants was performed as detailed in Spillane et al. (2011, 2012) and Donnelly et al. (2013).

(H) MitoTracker Green-labeled mitochondria (a and b) stalling at regions of ZBP1 accumulation at the base of filopodia. Seconds shown in panels. The region of the axon continuously populated by ZBP1 prior to the stalling of the mitochondrion (b) is denoted by the red bar at 0 and 260 s. Mitochondrion (b) is tracked by the green arrows between 100 and 260 s. Mitochondrion (a) stalled prior to the commencement of the shown sequence. Phase and ZBP1 shown at 0 and 260 s. (I) Example of an mt-DsRed-expressing axon segment with three mitochondria processed for β-actin mRNA FISH. Two of the mitochondria exhibit mRNA granules along their lengths (arrows) and one does not (arrowhead).

Constructs and Organelle Stains

The myrGFP constructs were the same as previously developed and used (Spillane et al., 2012). The mt-DsRed was provided by Dr. G. Smith (Temple University; Nasr et al., 2008). mCherry-ZBP1 was kindly provided by Dr. G. Bassell (Emory University; Nalavadi et al., 2012). GFP-L10A was provided by Dr. Y. Hu (Temple University), EB3-GFP as described in Ketschek and Gallo (2010), mt-KR was from Evrogen, and mt-GFP (pABCb10aa1-35-GFP) was from Addgene. Mitotracker and other dyes, all from Invitrogen, were prepared according to the manufacturer's directions. Mitotracker was used at 0.05 nM (red) and 25 nM (green); ER tracker and Lysotracker were used at 500 nM and 75 nM, respectively. Live cells were labeled with the dyes for 30 min in culturing medium, followed by three washes of medium prior to imaging.

Immunostaining, FISH, and Quantitative Analysis

Actin filaments and microtubules were stained using rhodamine-phalloidin (Invitrogen) and anti-α-tubulin DM1A-FITC (Sigma), respectively. For determination of branch formation (Figures 1F and 1G), cultures were simultaneously fixed (0.25% glutaraldehyde) and extracted (0.1% TX-100) in cytoskeletal buffer to only reveal polymeric cytoskeletal components, as described in Gallo and Letourneau (1998). Quantification of axonal microtubule content was performed using background subtraction as previously described (Spillane et al., 2012). The Y10B primary antibody (Abcam) was used at 1:200 and detected using secondary antibodies. For Y10B staining, cultures were fixed with 8% paraformaldehyde and subsequently permeabilized with 0.1% TX-100. FISH was performed using Stellaris probes from Biosearch Technologies (see Supplemental Information for details).

Branch Determination

In all experiments, we analyzed the distal 100 μm of axons. For Figures 1F and 1G and S2D and S2E, branches were defined as described in Spillane et al. (2012; see Figure S1A for details). For live-imaging experiments, the maturation of filopodia into branches was defined by (1) thickening and phase-contrast darkening of the filopodium and (2) the initiation of protrusive activity from the otherwise linear structure of the filopodium (Figures 1A and S1). This definition of branching identifies axonal protrusions that match the definition of branches used in the fixed preparation experiments based on the cytoskeletal definitions (compare Figure S1A to S1B and S1C).

Imaging and Analysis

Phase and wide-field epifluorescence imaging of live (dissociated, ganglion explants, and spinal cord explants) or fixed cells was performed on Zeiss Axiovert inverted microscopes equipped with heating stages for live-cell imaging (Spillane et al., 2012). For all live-cell imaging, cultures are allowed to equilibrate for 15 min on the heating stage prior to imaging. An Orca ER camera (Hamamatsu) was used for all wide-field image acquisition. For TIRF microscopy, we used a Zeiss system (Axio Observer Z1 inverted microscope) equipped with dual wavelength laser system (488 nm, 100 mW OPSL laser; 561 nm, 40 mW diode laser), an alpha plan-apo 100× 1.46 numerical aperture TIRF objective, and an Orca R2 camera (Hamamatsu). Quantitative analysis of images was performed using Zeiss Axiovision software. Line-scan analysis was performed using Image J. For details on the CALI of mt-KR, see Supplemental Information.

SUPPLEMENTAL INFORMATION

Supplemental Information includes Supplemental Experimental Procedures and six figures and can be found with this article online at http://dx.doi.org/10.1016/j.celrep.2013.11.022.

ACKNOWLEDGMENTS

This work was supported by the National Institutes of Health (R01-NS078030 to G.G. and R01-NS041596 to J.L.T.) and Dr. Miriam and Sheldon G. Adelson Medical Research Foundation (to J.L.T.). We thank Dr. G. Bassell (Emory University), Dr. G.M. Smith (Shriners Hospitals Pediatric Research Center), and Dr. Y. Hu (Shriners Hospitals Pediatric Research Center) for their kind gifts of reagents.

Received: June 24, 2013
Revised: September 30, 2013
Accepted: November 12, 2013
Published: December 12, 2013

REFERENCES

Aakalu, G., Smith, W.B., Nguyen, N., Jiang, C., and Schuman, E.M. (2001). Dynamic visualization of local protein synthesis in hippocampal neurons. Neuron *30*, 489–502.

Alvarez, J., Giuditta, A., and Koenig, E. (2000). Protein synthesis in axons and terminals: significance for maintenance, plasticity and regulation of phenotype. With a critique of slow transport theory. Prog. Neurobiol. *62*, 1–62.

Amiri, M., and Hollenbeck, P.J. (2008). Mitochondrial biogenesis in the axons of vertebrate peripheral neurons. Dev. Neurobiol. *68*, 1348–1361.

Aschrafi, A., Natera-Naranjo, O., Gioio, A.E., and Kaplan, B.B. (2010). Regulation of axonal trafficking of cytochrome c oxidase IV mRNA. Mol. Cell. Neurosci. *43*, 422–430.

Bulina, M.E., Chudakov, D.M., Britanova, O.V., Yanushevich, Y.G., Staroverov, D.B., Chepurnykh, T.V., Merzlyak, E.M., Shkrob, M.A., Lukyanov, S., and Lukyanov, K.A. (2006). A genetically encoded photosensitizer. Nat. Biotechnol. *24*, 95–99.

Ceci, M., Welshhans, K., Ciotti, M.T., Brandi, R., Parisi, C., Paoletti, F., Pistillo, L., Bassell, G.J., and Cattaneo, A. (2012). RACK1 is a ribosome scaffold protein for β-actin mRNA/ZBP1 complex. PLoS ONE *7*, e35034.

Chada, S.R., and Hollenbeck, P.J. (2003). Mitochondrial movement and positioning in axons: the role of growth factor signaling. J. Exp. Biol. *206*, 1985–1992.

Courchet, J., Lewis, T.L., Jr., Lee, S., Courchet, V., Liou, D.-Y., Aizawa, S., and Polleux, F. (2013). Terminal axon branching is regulated by the LKB1-NUAK1 kinase pathway via presynaptic mitochondrial capture. Cell *153*, 1510–1525.

Donnelly, C.J., Park, M., Spillane, M., Yoo, S., Pacheco, A., Gomes, C., Vuppalanchi, D., McDonald, M., Kim, H.H., Merianda, T.T., et al. (2013). Axonally synthesized β-actin and GAP-43 proteins support distinct modes of axonal growth. J. Neurosci. *33*, 3311–3322.

Gallo, G. (2011). The cytoskeletal and signaling mechanisms of axon collateral branching. Dev. Neurobiol. *71*, 201–220.

Gallo, G. (2013). Mechanisms underlying the initiation and dynamics of neuronal filopodia: from neurite formation to synaptogenesis. Int Rev Cell Mol Biol *301*, 95–156.

Gallo, G., and Letourneau, P.C. (1998). Localized sources of neurotrophins initiate axon collateral sprouting. J. Neurosci. *18*, 5403–5414.

Garden, G.A., Hartlage-Rübsamen, M., Rubel, E.W., and Bothwell, M.A. (1995). Protein masking of a ribosomal RNA epitope is an early event in afferent deprivation-induced neuronal death. Mol. Cell. Neurosci. *6*, 293–310.

Gibson, D.A., and Ma, L. (2011). Developmental regulation of axon branching in the vertebrate nervous system. Development *138*, 183–195.

Greif, K.F., Asabere, N., Lutz, G.J., and Gallo, G. (2013). Synaptotagmin-1 promotes the formation of axonal filopodia and branches along the developing axons of forebrain neurons. Dev. Neurobiol. *73*, 27–44.

Gu, W., Pan, F., Zhang, H., Bassell, G.J., and Singer, R.H. (2002). A predominantly nuclear protein affecting cytoplasmic localization of beta-actin mRNA in fibroblasts and neurons. J. Cell Biol. *156*, 41–51.

Hörnberg, H., and Holt, C. (2013). RNA-binding proteins and translational regulation in axons and growth cones. Front Neurosci *7*, 81–89.

Hörnberg, H., Wollerton-van Horck, F., Maurus, D., Zwart, M., Svoboda, H., Harris, W.A., and Holt, C.E. (2013). RNA-binding protein Hermes/RBPMS inversely affects synapse density and axon arbor formation in retinal ganglion cells in vivo. J. Neurosci. *33*, 10384–10395.

Kalous, A., Stake, J.I., Yisraeli, J.K., and Holt, C.E. (2013). RNA-binding protein Vg1RBP regulates terminal arbor formation but not long-range axon navigation in the developing visual system. Dev. Neurobiol.

Ketschek, A., and Gallo, G. (2010). Nerve growth factor induces axonal filopodia through localized microdomains of phosphoinositide 3-kinase activity that drive the formation of cytoskeletal precursors to filopodia. J. Neurosci. *30*, 12185–12197.

Lelkes, P.I., Unsworth, B.R., Saporta, S., Cameron, D.F., and Gallo, G. (2006). Culture of Neuroendocrine and Neuronal Cells for Tissue Engineering. In Culture of Cells for Tissue engineering, Chapter 14, G. Vunjak-Novakovic and R.I. Freshney, eds. (Hoboken: Wiley).

Lilley, B.N., Pan, Y.A., and Sanes, J.R. (2013). SAD kinases sculpt axonal arbors of sensory neurons through long- and short-term responses to neurotrophin signals. Neuron *79*, 39–53.

Mattson, M.P., Gleichmann, M., and Cheng, A. (2008). Mitochondria in neuroplasticity and neurological disorders. Neuron *60*, 748–766.

Nalavadi, V.C., Griffin, L.E., Picard-Fraser, P., Swanson, A.M., Takumi, T., and Bassell, G.J. (2012). Regulation of zipcode binding protein 1 transport dynamics in axons by myosin Va. J. Neurosci. *32*, 15133–15141.

Nasr, P., Sullivan, P.G., and Smith, G.M. (2008). Mitochondrial imaging in dorsal root ganglion neurons following the application of inducible adenoviral vector expressing two fluorescent proteins. J. Neurosci. Methods *172*, 185–194.

Onifer, S.M., Smith, G.M., and Fouad, K. (2011). Plasticity after spinal cord injury: relevance to recovery and approaches to facilitate it. Neurotherapeutics *8*, 283–293.

Sotelo-Silveira, J., Crispino, M., Puppo, A., Sotelo, J.R., and Koenig, E. (2008). Myelinated axons contain beta-actin mRNA and ZBP-1 in periaxoplasmic ribosomal plaques and depend on cyclic AMP and F-actin integrity for in vitro translation. J. Neurochem. *104*, 545–557.

Spillane, M., Ketschek, A., Jones, S.L., Korobova, F., Marsick, B., Lanier, L., Svitkina, T., and Gallo, G. (2011). The actin nucleating Arp2/3 complex contributes to the formation of axonal filopodia and branches through the regulation of actin patch precursors to filopodia. Dev. Neurobiol. *71*, 747–758.

Spillane, M., Ketschek, A., Donnelly, C.J., Pacheco, A., Twiss, J.L., and Gallo, G. (2012). Nerve growth factor-induced formation of axonal filopodia and collateral branches involves the intra-axonal synthesis of regulators of the actin-nucleating Arp2/3 complex. J. Neurosci. *32*, 17671–17689.

Steketee, M.B., Moysidis, S.N., Weinstein, J.E., Kreymerman, A., Silva, J.P., Iqbal, S., and Goldberg, J.L. (2012). Mitochondrial dynamics regulate growth cone motility, guidance, and neurite growth rate in perinatal retinal ganglion cells in vitro. Invest. Ophthalmol. Vis. Sci. *53*, 7402–7411.

Sun, T., Qiao, H., Pan, P.Y., Chen, Y., and Sheng, Z.H. (2013). Motile axonal mitochondria contribute to the variability of presynaptic strength. Cell Rep *4*, 413–419.

Tcherkezian, J., Brittis, P.A., Thomas, F., Roux, P.P., and Flanagan, J.G. (2010). Transmembrane receptor DCC associates with protein synthesis machinery and regulates translation. Cell *141*, 632–644.

Verburg, J., and Hollenbeck, P.J. (2008). Mitochondrial membrane potential in axons increases with local nerve growth factor or semaphorin signaling. J. Neurosci. *28*, 8306–8315.

Vuppalanchi, D., Willis, D.E., and Twiss, J.L. (2009). Regulation of mRNA transport and translation in axons. Results Probl. Cell Differ. *48*, 193–224.

Willis, D.E., van Niekerk, E.A., Sasaki, Y., Mesngon, M., Merianda, T.T., Williams, G.G., Kendall, M., Smith, D.S., Bassell, G.J., and Twiss, J.L. (2007). Extracellular stimuli specifically regulate localized levels of individual neuronal mRNAs. J. Cell Biol. *178*, 965–980.

Xing, L., Newbern, J.M., and Snider, W.D. (2013). Neuronal development: SAD kinases make happy axons. Curr. Biol. *23*, R720–R723.

Yoon, B.C., Jung, H., Dwivedy, A., O'Hare, C.M., Zivraj, K.H., and Holt, C.E. (2012). Local translation of extranuclear lamin B promotes axon maintenance. Cell *148*, 752–764.

Yu, H.Y., and Bement, W.M. (2007). Control of local actin assembly by membrane fusion-dependent compartment mixing. Nat. Cell Biol. *9*, 149–159.

Yudin, D., Hanz, S., Yoo, S., Iavnilovitch, E., Willis, D., Gradus, T., Vuppalanchi, D., Segal-Ruder, Y., Ben-Yaakov, K., Hieda, M., et al. (2008). Localized regulation of axonal RanGTPase controls retrograde injury signaling in peripheral nerve. Neuron *59*, 241–252.

Zala, D., Hinckelmann, M.V., Yu, H., Lyra da Cunha, M.M., Liot, G., Cordelières, F.P., Marco, S., and Saudou, F. (2013). Vesicular glycolysis provides on-board energy for fast axonal transport. Cell *152*, 479–491.

Zhang, H.L., Eom, T., Oleynikov, Y., Shenoy, S.M., Liebelt, D.A., Dictenberg, J.B., Singer, R.H., and Bassell, G.J. (2001). Neurotrophin-induced transport of a beta-actin mRNP complex increases beta-actin levels and stimulates growth cone motility. Neuron *31*, 261–275.